NASA-CR-172437

NASA Contractor Report 172437

Empirical Studies of Upper Atmospheric Species

John Nicholson, Mike Pitts and Dave Young

Systems and Applied Sciences Corporation
17 Research Drive
Hampton, VA 23666

Contract NAS1-17089
July 10, 1984

NASA
National Aeronautics and
Space Administration

Langley Research Center
Hampton, Virginia 23665

9 1 1 RN/NASA-CR-172437
DISPLAY 09/2/1
84N31847** ISSUE 21 PAGE 3443 CATEGORY 46 RPT#: NASA-CR-172437 NAS 1.26:172437 CNT#: NAS1-17089 84/07/10 39 PAGES UNCLASSIFIED DOCUMENT
UTTL: Empirical studies of upper atmospheric species TLSP: Final Report, 23 Jul. 1982 - 7 May 1984
AUTH: A/NICHOLSON, J.; B/PITTS, M.; C/YOUNG, D.
CORP: Systems and Applied Sciences Corp., Hampton, Va. AVAIL.NTIS SAP: HC A03/MF A01
MAJS: /*ATMOSPHERIC COMPOSITION/*COMPUTER PROGRAMS/*DATA PROCESSING/*SPACEBORNE EXPERIMENTS/*STRATOSPHERE/*THERMOSPHERE/*VENUS ATMOSPHERE
MINS: / ATMOSPHERIC DENSITY/ ATMOSPHERIC MODELS/ ATMOSPHERIC TEMPERATURE/ DYNAMICS EXPLORER SATELLITES/ NIMBUS SATELLITES/ NITRIC ACID/ NITROGEN DIOXIDE/ OZONE/ PIONEER VENUS SPACECRAFT
ABA: Author
ABS: The first month of spin-scan ozone imaging (SOI) data (October 1981) was processed and compared with total ozone mapping spectrometer and ground based data. Short term variations in the ozone field have been revealed using animated sequences of SOI data. High correlations were observed between SOI ozone and upper tropospheric meteorological data. The relationship between ozone and temperature in the stratosphere was investigated by examining Nimbus 4 backscattered ultraviolet ozone and selective chopper radiometer temperature measurements as well as solar
ENTER:

TABLE OF CONTENTS

1 - INTRODUCTION

This document is the final report for contract NAS1-17089 for the time period beginning July 23, 1982 and ending May 7, 1984. During this period, Systems and Applied Sciences Corporation developed for the National Aeronautics and Space Administration (NASA), Langley Research Center (LaRC) some of the computer programs for processing and analyzing atmospheric data from experiments aboard Earth and Venus orbiting spacecraft. The experiments were the Spin-Scan Ozone Imaging (SOI) Experiment on the Dynamics Explorer Spacecraft (DE-I), the Backscatter Ultraviolet (BUV) and Selective Chopper Radiometer (SCR) Experiments on Nimbus 4, the Solar Backscatter Ultraviolet (SBUV), the Stratospheric and Mesospheric Sounder (SAMS) and the Limb Infrared Monitor of the Stratosphere (LIMS) Experiments on Nimbus 7, and the Orbiter Atmospheric Drag (OAD) Experiment on the Pioneer Venus Orbiter Spacecraft. The computer programs were then used to perform collaborating studies with LaRC scientists for the determination of the distribution in the Earth's atmosphere of total columnar ozone (total ozone) from SOI, ozone mixing ratio (ozone) and temperature from BUV and SBUV, and SCR and SAMS respectively, nitric acid (HNO_3), nitrogen dioxide (NO_2) and water (H_2O) mixing ratios from LIMS, methane (CH_4) and nitrous oxide (N_2O) mixing ratios from SAMS, and the Venus atmospheric densities from OAD.

2 - SPIN-SCAN OZONE IMAGING EXPERIMENT

Data reduction, validation, and analysis of total column ozone (total ozone) data from the Dynamics Explorer I (DE-I) Spin-Scan Ozone Imaging (SOI) Experiment is in progress. This experiment measures total ozone using the backscattered ultraviolet (BUV) technique similar to that used on Nimbus 4 and 7. Measurements of backscattered sunlight are made at 317.5 nm and 360.0 nm using the Spin-Scan Imaging Instrumentation on DE-I. The spin of the DE-I spacecraft, coupled with a laterally scanning mirror enables a global-scale image of the total ozone field to be produced in twelve minutes or less dependent upon the size of the image. Additionally, the DE-I satellite is in a highly eccentric polar orbit. This not only allows continuous global-scale total ozone images for hours at a time while the satellite is near apogee (~23,000 km), but also permits high resolution (~3 km) images of the total ozone field while near perigee.

Some of the SOI data for October, 1981 has been processed. Data-blocking and modeling software developed for prior empirical modeling studies has been modified for use in validating and analyzing these data.

In addition, new software has been refined for producing synoptic, pseudo-color images of the total ozone field. These images are an important, qualitative tool for the study of short-term total ozone variations and can be animated to produce films of the evolving total ozone field. Since these images are

synoptic, they can be compared directly with synoptic meteorological data in order to demonstrate the relation between the total ozone distribution and atmospheric dynamics near the tropopause.

During this contract, the emphasis of the SOI data analysis has been: 1) comparing SOI data with the Total Ozone Mapping Spectrometer (TOMS) on the Nimbus 7 spacecraft and ground-based Dobson data to assure the accuracy of the SOI data; 2) comparing synoptic SOI images with asynoptic TOMS data in order to study short-term variations in the total ozone field; and 3) studying the correlation between SOI total ozone and upper tropospheric synoptic data in order to establish the meteorological applications for this data set.

Approximately 2800 SOI radiance data images measured during the time period September 29 to November 14, 1981 have been catalogued, copied, and archived on magnetic tape. From this data base more than 750 total ozone images have been produced. The total ozone data have also been catalogued and archived on magnetic tape at NASA Langley Research Center.

The software for reading, displaying, and blocking both the radiance data tapes and the total ozone data tapes has been refined and is currently operational. The blocking routines, which group and average the data onto a 2^{o} latitude by 2^{o} longitude grid, are used in order to more practically handle the large amount of data. Once the data are blocked, reblocking (either into a coarser grid or using running means) and displaying the data is vastly simplified and less expensive.

The total ozone data reduction and co-location programs have been incorporated into the NASA-Langley computer system. Included with these programs are the tables of theoretical 317.5 nm and 360.0 nm albedos, slant path, and terrain height necessary for the calculation of total ozone.

One of the principal goals of this research has been the validation of the SOI total ozone measurements. Prior to this work, validation had consisted solely of comparisons of 15th order-15th degree spherical harmonic models of the SOI total ozone data with ground-based Dobson measurements from the time period September 29 - October 3, 1981. The comparison between the two data sets was excellent, with a standard deviation of less than 3% for all weather conditions excluding rain.

Comparisons have now been performed between SOI and TOMS. The TOMS data is particularly advantageous for use in validating SOI total ozone measurements. First of all, both SOI and TOMS use backscattered ultraviolet techniques for measuring total ozone and can thus be directly compared. In addition, global TOMS total ozone data are available for October, 1981 so that same-day comparisons can be made. However, since the TOMS experiment produces global images by piecing together data from many orbits, only a portion of each TOMS image will contain concurrently measured SOI data. Thus, although TOMS represents the best available data set for validating SOI, care has been taken concerning time differences when direct comparisons have been made.

Software has been developed to perform this comparison.

Programs have been designed to: 1) read the TOMS data tapes and block the data into 2^{o} latitude by 2^{o} longitude cells; 2) reblock the SOI data using running means; and 3) reblock, correlate, and plot the two data sets.

The reblocking software has been used to study the quality of the SOI data. It has been demonstrated that hourly averaged, 6^{o} x 6^{o} running means of the SOI total ozone values reveal data comparable to the 2^{o} x 2^{o} TOMS data. All comparisons have been performed using this degree of smoothing.

The correlation and plotting routines were used to search for biases between the two data sets. This study has led to the detection of the following trends:

1. A constant bias in ozone of 8% assumed due to the different values of the ozone absorption coefficient used by SOI and TOMS in the ozone retrieval algorithm.
2. A latitudinal relative bias in reflectivity.
3. Increased discrepancies between ozone values at low solar zenith angles.
4. A significant east-west relative bias in ozone at all latitudes;

Of these, 4 appears to be the most serious. A similar problem has been reported by another experimenter using the photometers aboard DE-I. A correction for the east-west relative bias has been modeled and incorporated in the blocking routine.

Since the geographical extent of an SOI image can be duplicated only by combining 3 to 4 TOMS orbits spaced approximately 2 hours apart, only one of the orbits can be at the

exact time of the SOI scene. The best agreement between SOI and TOMS data occurs in the regions of concurrent measurements. In other portions of the SOI image, apparent changes in the total ozone field have occurred during the 1-4 hour interval between the TOMS measurements.

The occurrence of small-scale variations in the total ozone field on this time scale has been confirmed by animating a sequence of SOI images from October 2, 1981. The sequence includes data taken in 12-minute increments and spans approximately three hours. Significant (~12 Dobson Units) increases in total ozone occur during this time interval in two regions: 1) directly ahead of a strong cold front and its associated squall line as determined from meteorology charts and 2) in a region of clear air surrounded by strong convection in the tropics as seen in the Geostationary Orbiting Environmental Satellite scenes. These features imply a possible connection between increasing total ozone and regions of compensating subsidence near strong convection. This appears to be an extension to a smaller scale of the observed inverse relationship between total ozone and tropopause height (which shall be described below).

Another interesting small-scale feature revealed by animating the SOI images is an area of high total ozone that appears to be spinning off from a northerly jet stream. This feature seems to be indicative of an eddy in the upper air flow created by shear on the anti-cyclonic side of the jet.

The animated sequence has been presented at NASA Langley,

NASA Goddard, NASA Headquarters and at the National Center for Atmospheric Research, Boulder, Colorado. Interest has been expressed in applying these data in studies by mesoscale modelers and in conjunction with airplane in-situ measurements of tropospheric folds.

Another avenue of data analysis that has been pursued is the correlation of total ozone with other meteorological parameters such as the location of the jet stream and the latitude of the tropopause. Some results of this study which were presented at a meeting at NASA Goddard on April 16, 1984 entitled, "Potential Meteorological Uses of Total Ozone Data" are as follows.

It has been demonstrated since the advent of Dobson ground station measurements of total ozone that there is a relation to total ozone and the location of the jet stream as well as a strong negative correlation with tropopause altitude. The purpose of this study was to determine whether these relationships hold for the small spatial and time scales observed by SOI.

As a qualitative example, Figure 1 shows the relationship between SOI ozone horizontal gradients and the wind speed contours of 75 and 100 knots obtained from the 250 millibar constant pressure meteorology chart for October 24, 1981. The jet stream is defined as the area where wind speeds are greater than 75 knots. As can be seen in the figure, the highest winds occur in areas of the largest horizontal gradient of total ozone. The slight displacement of the winds to the east is most likely due to the difference in times of observation. This non-

simultaneity of measurements is a problem in all of these studies: however, this does point out a possible advantage of SOI data. If the correlation between total ozone and tropopause altitude is valid, then the synoptic SOI images may be a valuable aid in providing upper tropospheric wind speed information at times not measured by the upper-air sounding network.

The variation of SOI total ozone and tropopause altitude with longitude at two latitudes over North America on October 2, 1981 is shown in Figure 2. In both cases, a linear regression analysis indicated that a strong negative correlation exists between total ozone and tropopause altitude of better than -0.89. Such highly negative correlations are generally observed when only tropopause data over land is used. When tropopause data taken over water by satellites is included, the correlation is reduced by approximately 30 percent. This is indicative of the difference in tropopause altitude estimates from radiosonde and satellite measurements.

Another feature of this correlation is seen in Figure 3, where the variation of correlation coefficients between the locations of the minimum values of total ozone and the maximum values of tropopause altitude over North America on October 1 and 2, 1981 is presented. The correlation is quite high (-0.95) in mid latitudes and falls off appreciably at lower latitudes. Although this may be due in part to the decrease in radiosonde coverage in this region, there are indications that this may indeed be a real effect.

Future work should focus on using the actual radiosonde data

in the correlations instead of the smoothed tropopause altitude charts. This will enable closer inspection of the data, including the possibility of taking double tropopauses and folds into consideration. The actual radiosonde data will also provide useful meteorological assistance in analyzing the total ozone data such as the use of isentropic cross sections for locating tropopause folding events.

Finally, measurement strategy planning for SOI should continue. As more users of these data are identified, it will become increasingly important to assure the acquisition of as much relevant data as possible. Thus, a continual monitoring of the instrument's viewing conditions and frequent communication with the University of Iowa should be maintained in order to optimize the planning of the measurement strategy.

3 - OZONE-TEMPERATURE RELATIONSHIP

The relationship between ozone mixing ratio (ozone), ratio of ozone density to air density, and temperature in the stratosphere has been investigated by examining simultaneous ozone and temperature satellite observations at various latitudes and altitudes. Analysis of correlation and regression coefficients of ozone and temperature provides information about the sensitivity of ozone to temperature in the stratosphere. In general, positive correlations are expected to be found in the lower stratosphere where ozone and temperature are in phase. A transition from positive to negative correlations, associated with the shift from dynamical control to photochemical control, is expected above 30 km (~10 mb). Strong negative correlations are expected above this transition region indicating photochemical control. Regression coefficients of the natural logarithm of ozone and temperature represent the sensitivity of the ozone to temperature changes and are expressed as the percent change in ozone per degree K decrease in temperature.

Ozone measurements from the Nimbus 4 solar backscatter (BUV) experiment and temperature measurements from the Nimbus 4 selective chopper radiometer (SCR) experiment have been analyzed, as well as ozone measurements from the Nimbus 7 solar backscatter ultraviolet (SBUV) experiment and temperature measurements from the Nimbus 7 stratospheric and mesospheric sounder (SAMS). Results from these ozone-temperature studies have been compared with calculations from theoretical 2-D models.

3.1 Satellite Data.

The BUV data set utilized in this study consists of ozone profiles measured along each orbit at various latitudes between 80°N and 80°S. Each profile contains mixing ratios at 13 pressure levels: 40, 30, 15, 10, 7, 6, 5, 4, 3, 2, 1.5, 1 and .7 mb. The SCR data was initially received as daily latitude-longitude grids of radiance profiles with 36 elements in longitude (every 10°) and 41 elements in latitude (every 4° from 80°N to 80°S). Each SCR profile contains radiance values at height intervals of 0.2 in log to the base e (ln) pressure from near the surface up to approximately 50 km. The radiance measurements were converted to temperatures, then, in order to match up better with the BUV data, the temperatures were interpolated to the 13 BUV pressure levels.

The SBUV data set consists of ozone profiles measured along each orbit at various latitudes. Each profile contains mixing ratios at 16 pressure levels: 40, 30, 20, 15, 10, 7, 5, 4, 3, 2, 1.5, 1.0, 0.7, 0.5, 0.4 and 0.3 mb. The SAMS temperature data was received as daily latitude-longitude grids at height intervals of 0.2 in ln pressure from near the surface up to approximately 90 km. The latitude-longitude grids have 48 elements in latitude (every 2.5° from 50°S to 67.5°N) and 36 elements in longitude (every 10°). The temperature grids were interpolated to the 16 SBUV standard pressure levels.

In order to calculate statistics, the ozone and temperature data have been blocked into latitude-longitude cells by day. The BUV ozone and SCR temperature data have been blocked into 4°

latitude by 10^{o} longitude cells at each of the 13 BUV standard pressure levels for every day of available data from October 1970 through March 1972. The SBUV ozone and SAMS temperature data have been blocked into 5^{o} latitude by 10^{o} longitude cells at each of the 16 SBUV standard pressure levels for every day of available data from October 1978 through October 1979. Correlation and regression coefficients have been calculated for each latitude belt at each pressure level for every month of blocked data.

Analysis of the correlation coefficients between longitudinal variations of BUV ozone and SCR temperature data has revealed large regions of strong negative correlations. These areas of strong correlations are mainly present in the middle and high latitudes above approximately 40 km. Strong correlations are observed in both hemispheres during spring and fall months, but are confined mainly to the winter hemisphere at other times of the year.

Analysis of the regression coefficients between longitudinal variations of BUV ozone and SCR temperature data has revealed a distinct ridge of maximum sensitivity. The altitude of the ridge, which is located near the stratospause, exhibits both longitudinal (wave effects) and seasonal variations. The altitude increases toward the poles from the equator and is higher in winter than in other seasons. The magnitude of the regression coefficients increases along the ridge toward the equator. The average sensitivities are approximately 1.7% per ^{o}K. The regression coefficients have been analyzed only in

regions of high correlation ($|r| \geq 0.7$) in order to strengthen the level of confidence. The regression coefficients for the month of March 1971 are depicted in Figure 4.

Regions of high correlation between ozone and temperature, where results have a higher level of confidence, are limited to extratropical latitudes when examining longitudinal variations because of the lack of wave activity in the tropics. However, since high correlations in the zonal means are not limited by wave activity, the ozone-temperature relationship can be studied at all latitudes. Correlation and regression coefficients have been calculated between variations in the zonal means of BUV ozone and SCR temperature data. Results using the variations in the zonal means are similar to the results using longitudinal variations.

Nimbus 7 SBUV ozone and SAMS temperature data for the year 1979 has been analyzed. Correlation and regression coefficients have been calculated between variations in the zonal means of the SBUV-SAMS blocked data. Examination of these new data supports the results of the BUV-SCR studies. However, the magnitude of the sensitivities calculated with the SBUV-SAMS data are smaller than the magnitude of the BUV-SCR sensitivities. The regression coefficients obtained from the Nimbus 7 data for 12/24/78 - 2/8/79 are shown in Figure 5.

3.2 Theoretical Model Data.

Theoretical studies of the ozone sensitivity to temperature have been performed using 2-D models. Calculations from these

models have been compared with results from satellite observations. The model calculations have been interpreted only above approximately 10 mb because the dynamically controlled regions are not modeled adequately with photochemical models. One of these studies had been performed using the NASA-Ames 2-D model. The Ames model was run for a spring-fall case (March). The results show an apparent ridge of maximum sensitivity. In agreement with satellite data, the altitude of the ridge increases from the equator to the poles. However, the altitude of the ridge is higher than observed in satellite data and the maximum sensitivities along the ridge are substantially smaller. Another study was performed using the Pyle et al. 2-D model. The Pyle et al. model also indicates a ridge of maximum sensitivity. As in the Ames model, the latitudinal variation of the Pyle et al. model's ridge agrees well with variations in the satellite data. However, the altitude of the ridge is also higher than observed in satellite data and the magnitude of the maximum sensitivities along the ridge are less. Typical computations of the variation of ozone mixing ratio per degree kelvin decrease in temperature from the Pyle model are shown in Figure 6.

Theoretical studies on the effect of $C\ell O_x$, NO_x, and HO_x chemistry on the ozone-temperature relationship have also been performed. The results of these model calculations indicate that the principal chemistry controlling the ozone sensitivity to temperature near the ridge is O_x and $C\ell O_x$. HO_x chemistry appears to become increasingly important above the ridge but makes

significant contributions only at high latitudes where the ridge altitude is higher. Also, it is apparent that NO_x chemistry is significant only at altitudes considerably below the ridge. These results are shown in Figure 7.

In an effort to explain the differences between theoretical calculations and satellite observations, several variations of the basic model runs have been compared with satellite data. Theoretical calculations have been performed with the Pyle et al. model using ambient temperatures instead of an isothermal atmosphere. Results from these calculations depict a ridge of maximum sensitivity that is more comparable in shape to the satellite data than the basic model run. Since the 2-D model calculations have predicted $C\ell O_x$ chemistry to be important in controlling the ozone sensitivity near the ridge altitudes, the models were run with no $C\ell O_x$ chemistry included in the calculations. Interestingly, the model calculations without $C\ell O_x$ chemistry compare better with satellite observations than previous model runs. Without $C\ell O_x$ chemistry included, the model predicts a ridge which is both lower in altitude and higher in magnitude than the model basic runs. Figure 8 shows observed and predicted ozone sensitivities.

The ridge of maximum sensitivities, apparent in theoretical calculations as well as observations, may be the result of several contributing factors. The lower stratosphere is controlled by dynamics and in this region ozone exhibits little temperature dependence. Therefore, below the ridge, sensitivities are low. Above the ridge, HO_x chemistry lowers the

temperature dependence of ozone and hence lowers the sensitivities. However, dynamical effects are stronger in middle and high latitudes and extend to higher altitudes than in equatorial regions. Therefore, the bottom side of the ridge is eroded away by these dynamical effects causing the ridge to appear as if it sloped upward toward the poles. The maximum sensitivities along the ridge decrease with increasing latitude because of increased dynamical effects shifting the ridge to higher altitudes where greater HO_x effects occur. Since dynamical effects are strongest during winter months, the ridge would be eroded away more in winter. Therefore the ridge would appear higher in altitude during winter months.

When sensitivities calculated from satellite observations are compared with the theoretical model results several conclusions may be drawn. Both models depict a ridge of maximum sensitivity, but their ridges are higher in altitude and the sensitivities are smaller in magnitude than observed. The theoretical models show that when chlorine is effectively removed from their ambient atmospheres the ridge altitude is lowered and the magnitude of the sensitivities along the ridge are increased. The model results, therefore, compare more favorably with the observations when chlorine concentrations are significantly reduced in the calculations. This would imply that the difference between the observed and predicted sensitivity near the ridge would be reduced if (1) the effect of $Cl O_x$ on O_3 losses is substantially less than predicted, or (2) the temperature dependence of $Cl O_x$ chemistry on O_3 is much greater

than generally assumed. Furthermore, observations show that the sensitivity of ozone (O_3) to temperature has decreased over the period from 1972-1979. If ClO_x concentrations in the stratosphere have increased over this same time period, the resulting decrease in sensitivity might be similar to that observed.

4 - DATA SETS OF OTHER ATMOSPHERIC SPECIES

4.1 Limb Infrared Monitor of the Stratosphere (LIMS).

All of the LIMS data (Nov., 1978 - May, 1979) has been blocked into daily averages. Each day block contains data for 37 latitudes (-62^{o} to $+82^{o}$ in 4^{o} increments), 10 pressure levels (.05, .1, .2, .5, 1.0, 2.0, 5.0, 10.0, 20.0, and 50.0 mb), and for 10 combinations of 2 measured quantities (for correlation purposes) (T-$\ell n(O_3)$, T-$\ell n(H_2O)$, T-$\ell n(HNO_3)$, T-$\ell n(NO_2)$, O_3-H_2O, O_3-HNO_3, O_3-NO_2, H_2O-HNO_3, H_2O-NO_2, and HNO_3-NO_2). Each of these combinations contains both day and night averages of the 2 quantities, their variances, and the total number of points. Monthly correlations have been performed and the day and night resultant correlation and regression coefficients have been tabulated for pressure level versus latitude. Similar tabulations exist for averages, variances, variance/average, and number of points for the five quantities measured - T, O_3, H_2O, HNO_3, and NO_2.

Expansions of $\ell n(O_3)$ in such terms as $A + BT + C\ \ell n(H_2O) + D\ell n(HNO_3) + E\ell n(NO_2)$ have been done for each latitude band for day and night where a sufficient number of days of good data (data in which all of the variables were present) existed. These expansions were made thus far for only 2 mb and 5 mb. It is hoped that the coefficients and their respective errors in these various expansions will aid future work in understanding the importance of various chemical reactions in this pressure region.

4.2 Stratospheric and Mesospheric Sounder (SAMS).

SAMS daily zonal means for CH_4 and N_2O mixing ratios during 1979 have been received from Oxford University, England and the data have been interpolated into 8 pressure levels (.2, .5, 1.0, 2.0, 5.0, 10.0, 20.0, and 50.0 mb) at 48 latitudes (-50.0^{o} to 67.5^{o} every 2.5^{o}) along with their respective errors for each day. Since the SAMS instrumentation cannot measure CH_4 and N_2O simultaneously, each daily block usually contains only one of the two.

Since CH_4 and N_2O mixing ratios are desired along with the quantities measured by LIMS (Temperature and O_3, H_2O, HNO_3, and NO_2 mixing ratios) for comparison with theoretical model predictions, two additional programs have been devised for an initial test period (April 1-5, 1979). One of these is simply a temporal interpolation program to fill in the missing days for each of the two, CH_4 and N_2O. The other interpolates the CH_4 and N_2O data into latitude bands common with the LIMS data. (LIMS have 62^{o} to 82^{o}, every 4^{o}; SAMS have -50^{o} to 67.5^{o}, every 2.5^{o} - so that the output interpolated SAMS data have -50^{o} to 66^{o} every 4^{o} - 30 levels total).

5 - PIONEER VENUS ORBITER

The orbiter Atmospheric Drag Experiment utilizes the Pioneer Venus Orbiter spacecraft as an "instrument" in that the basic data for the experiment is the observed changes in the period of the spacecraft orbit caused by atmospheric drag acceleration. Period changes are determined by comparison of successive orbit solutions obtained from tracking data. Doppler data from the Deep Space Network (DSN) is input to an orbit fitting program which determines an orbit whose computed Doppler values most closely match the observed Doppler from the DSN. The observed period changes are the result of all non-conservative forces acting on the spacecraft; i.e., atmospheric drag, solar radiation pressure, n-body perturbations, etc. The significant perturbations other than atmospheric drag can be modeled to a high degree of accuracy and are subtracted from the total to yield the net effect due to drag. The resulting net orbital decay rate is combined with knowledge of the spacecraft mass, projected area, drag coefficient, and upper atmospheric model to yield atmospheric densities. These densities are referred to an altitude equal to one-half scale height above periapsis which reduces errors caused by uncertainties in composition and temperature of the assumed atmospheric model. The density data inferred from drag effects are then used to update and refine the Venus upper atmosphere model and to study the spatial and temporal variations of density.

A definite effect of solar flux upon the Venusian upper

atmospheric temperature and composition has been identified.

During this contract, most of the effort in regards to the Pioneer Venus Orbiter has been directly or indirectly concerned with the preparation of material for the Venus International Reference Atmosphere (VIRA). Two workshops have been held for VIRA, the first in Hamburg, West Germany during August 1983, and the second in Graz, Austria, June-July 1984. The main thrusts of the investigator's work has been the updating of the Venus Orbiter Atmospheric Drag (OAD) model, its comparison with other existing models, aiding in development of new models (especially theoretical models) of the Venus thermosphere, and the inclusion of the existing models as well as the new models into the OAD model.

5.1 Updating of the Venus Orbiter Atmospheric Drag (OAD) Model.

After examination of more recent work by Seiff, it appeared that our original assumption of a constant pressure at 115.1 km above the Venusian surface at all local solar times was not valid. His results would indicate a constant pressure region at about 100 km to be more reasonable. Secondly our shape parameter, s, originally assumed to be .069 was changed to .2 at night (still .069 during the day) to better fit the experimental data. Next total number densities of molecular mass 28 ($CO + N_2$) at 167 km as determined by the Orbiting Neutral Mass Spectrometer (ONMS) were employed to obtain better values of turbopause heights, mixing ratios of atomic oxygen and molecular mass 28 ($CO + N_2$) at the turbopause, and exospheric temperatures at various

times of day from the OAD model. Whereas the results of this model were generally in agreement with observations of other experimenters over it's valid altitude range (above 140 km), the model did seem to be sensitive to the assumptions made at 100 & 167 km.

After considering various approaches, it was decided to compare other models with OAD with more scrutiny than previously done to determine just what changes in each would be necessary to bring all into agreement, determining if possible what combination and/or hybrid would produce the most satisfactory results.

5.2 Comparison of OAD with other Models.

The most significant comparison work was done between OAD and an empirical model of the Venus thermosphere published in the Journal of Geophysical Research by Hedin et al. This model is based upon measurements made by the Orbiting Neutral Mass Spectrometer (ONMS) and yields temperature, total mass density, and number densities of CO_2, O, CO, He, N, and N_2 as a function of altitude, local solar time, latitude, and $F_{10.7}$ (the measurement of solar activity).

It should be again stressed that this is an empirical model; this point is further emphasized by the fact that the number densities as measured by the mass spectrometer had to be multiplied by a factor of 1.63 to bring them into agreement with other experimenters. However this seemed to be a simple bias and the precision of mass spectrometer measurements appeared good.

The $F_{10.7}$ cm tables used in the Hedin et al. model were those at 1 AU, not those calculated at Venus (as done in the OAD model) so a new table had to be constructed. In this model the phase angle of the Venus-Sun line relative to the Earth-Sun line was taken into consideration as in the OAD model, but the effect of the slight ellipticity of Venus' orbit was not considered. Although small, this effect was taken into consideration in the investigator's programming of the Hedin model. These changes, although small, produce a more exact model.

After the programming of Hedin's model was checked (this took quite some time due to various inaccurate expressions in the JGR text), it was compared with the OAD model - total density, number densities of atomic oxygen, molecular mass 28, and CO_2 as a function of altitude, local solar time, and $F_{10.7}$ flux. There were, of course, some differences, but generally agreement was good. The OAD densities at 150 km were numerically integrated in 1 km steps down to 100 km using various s parameters and temperature profiles with the aim of reproducing Massie and Hunten's, Seiff's, and Taylor's densities at 100 km. Once satisfactory results were obtained, this model using OAD assumptions from 100-150 km was incorporated into the modified OAD model from 150-350 km (to be discussed subsequently) for consideration at the first VIRA workshop held in Hamburg, West Germany during August, 1983.

It was decided to determine various quantities and combinations thereof in the ONMS model using OAD drag data. These included multipliers of the various constituents (each

empirical multiplier was no longer constrained to 1.63 as mentioned before), the average exospheric temperature, 1st - 5th order dependence of the average exospheric temperature upon local solar time and solar zenith angle, its dependence upon daily and 81 day average values of the $F_{10.7}$ flux, and the dependence of the atomic oxygen concentration upon the daily and 81 day average flux. Table 1 summarizes our results in this determination.

5.3 Inclusion of Other Models into the OAD Model.

It was decided that the following model be produced for consideration at the Hamburg, West Germany VIRA meeting. The ONMS model was used along with OAD drag data as just explained to solve for various coefficients (constituent multipliers, average exospheric temperature,...). The ONMS model with these coefficients was used to predict "base" temperatures and constituent concentrations for various local solar times at a specified altitude--in this case 150 km. The dependence of the temperature and the concentration of each constituent with altitude and local solar time was then assumed to be that predicted by the updated OAD model. As stated before, this model along with the numerical integration model from 100-150 km was presented at the Hamburg meeting. This model listed predicted values from 100-250 km of the following quantities: total density, number densities of CO_2, O, CO, He, N, N_2, and H; mean molecular weight; total number density; pressure; speed of sound; mean free path; pressure scale height; and density scale height. Plots of dayside (local solar time - noon) and nightside

(local solar time - midnight) can be seen in figures 9 and 10. These display the concentrations of the various constituents as well as total density, ρ, as a function of altitude.

5.4 New Theoretical Models.

A model similar to that presented at Hamburg was developed with the main difference being its complete symmetry. (Temperature, total density, number densities of all constituents,... were all symmetric with respect to local solar time). This model served as the basis of a new theoretical model developed by Bougher and Dickinson of the Venus thermosphere taking into account the most recent knowledge of heating, heat conduction, and radiative-absorption efficiencies as well as predicted dynamics in this region. Preliminary results show that the theoretical model is close to the modified OAD model. The major differences occur in CO and He predictions at midnight at 150 km and CO and He predictions at 100 km at both noon and midnight. These discrepancies are currently being investigated.

Orbits of high and low solar flux on Venus are being examined by Dr. Jane Fox of the Smithsonian Astrophysical Observatory. Typical high and low solar flux orbits have been chosen, and their respective $F_{10.7}$ flux on Venus, temperature including $F_{10.7}$ flux according to the OAD model, temperature without $F_{10.7}$ flux, and vertical composition profiles have been sent to her. Her theoretical model will be evaluated for these orbits and compared to the OAD model.

TABLE 1.

MODEL PARAMETERS DERIVED FROM OAD DRAG DATA AND ONMS 150 KM MIXING RATIOS

Composition Sensitivity Parameters

CO_2 multiplier	1.83
O multiplier	1.58

Mean Exospheric Temperature (^0K)

$\overline{T}_\infty$	229.1

Solar Activity Temperature Parameter $(10^{-22} Wm^{-2} Hz^{-1})^{-1}$

F_{10} parameter	0.084×10^{-2}

Diurnal Temperature Parameters

a_{10}	+0.592
b_{11}	-0.175
a_{20}	-0.063
b_{22}	-0,015
a_{30}	-0.234
b_{33}	$+0.016 \times 10^{-1}$
a_{40}	+0.024
b_{44}	-0.015×10^{-2}
a_{50}	+0.036
b_{55}	$+0.034 \times 10^{-3}$

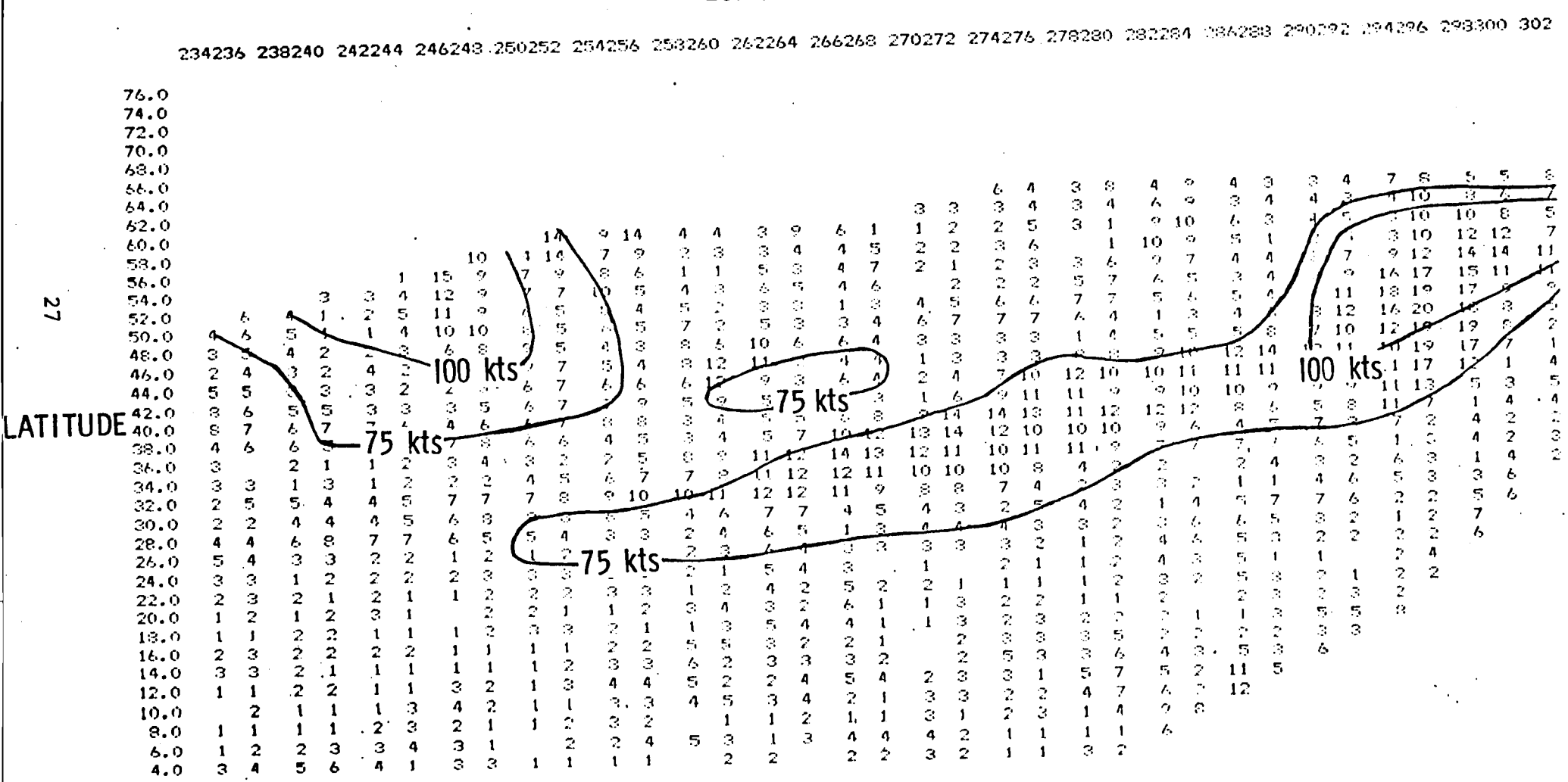

Figure 1. The comparison of SOI total ozone gradients (Dobson Units/degree latitude) with the location from 250 millibar constant pressure meteorology charts of the jet stream on October 24, 1981.

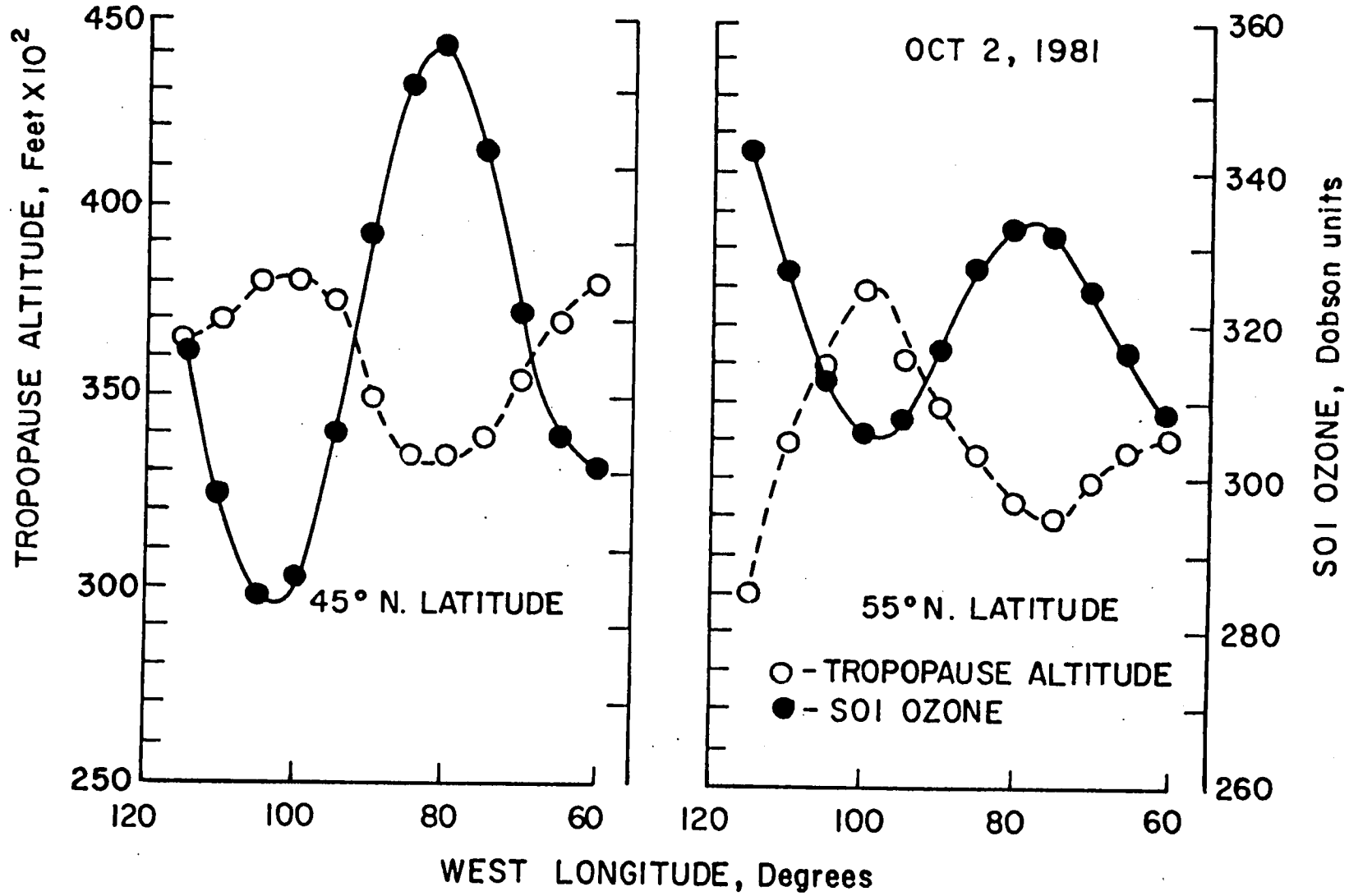

Figure 2. The variation of SOI total ozone and tropopause altitude with longitude at two latitudes over North America on October 2, 1981.

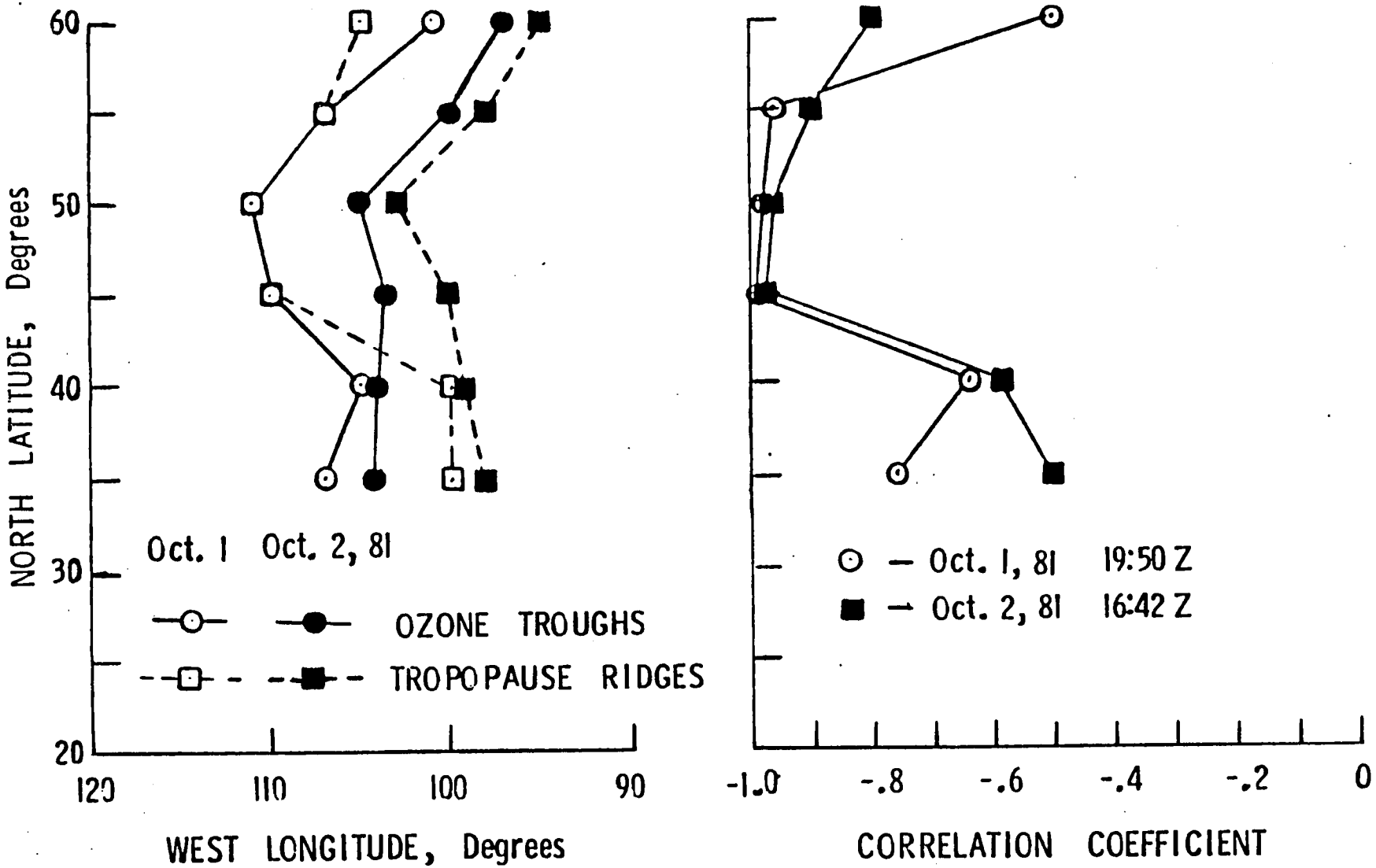

Figure 3. The variation of the correlation coefficient between the location of the minimum values of total ozone (troughs) and the maximum values (ridges) of tropopause altitude over North America on October 1 and 2, 1981.

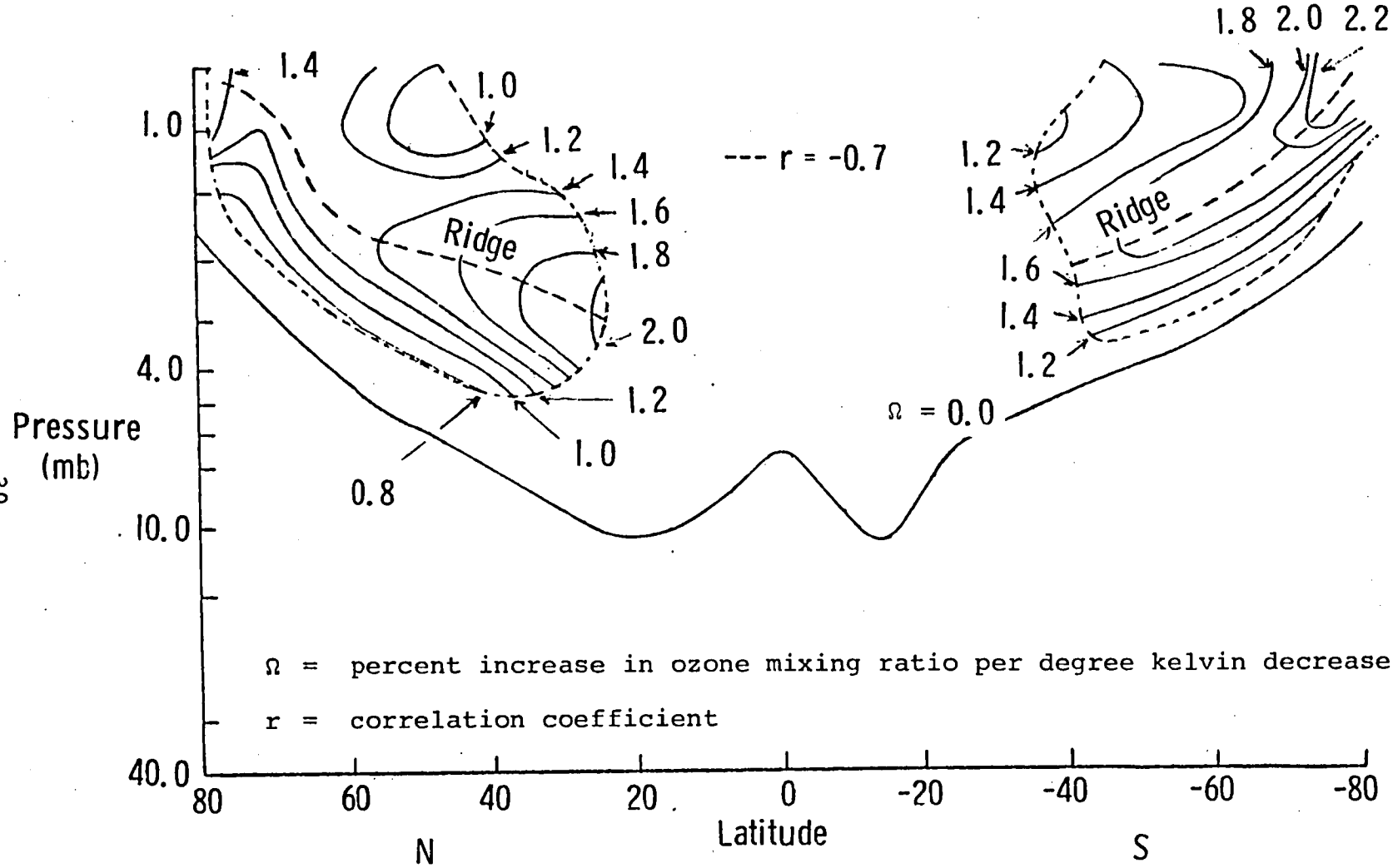

Figure 4. The percent increase in ozone mixing ratio per degree kelvin decrease in temperature (regression coefficients) as a function of latitude and pressure height for correlation coefficients $\geq$ -0.7 obtained from Nimbus 4 observations in March 1971.

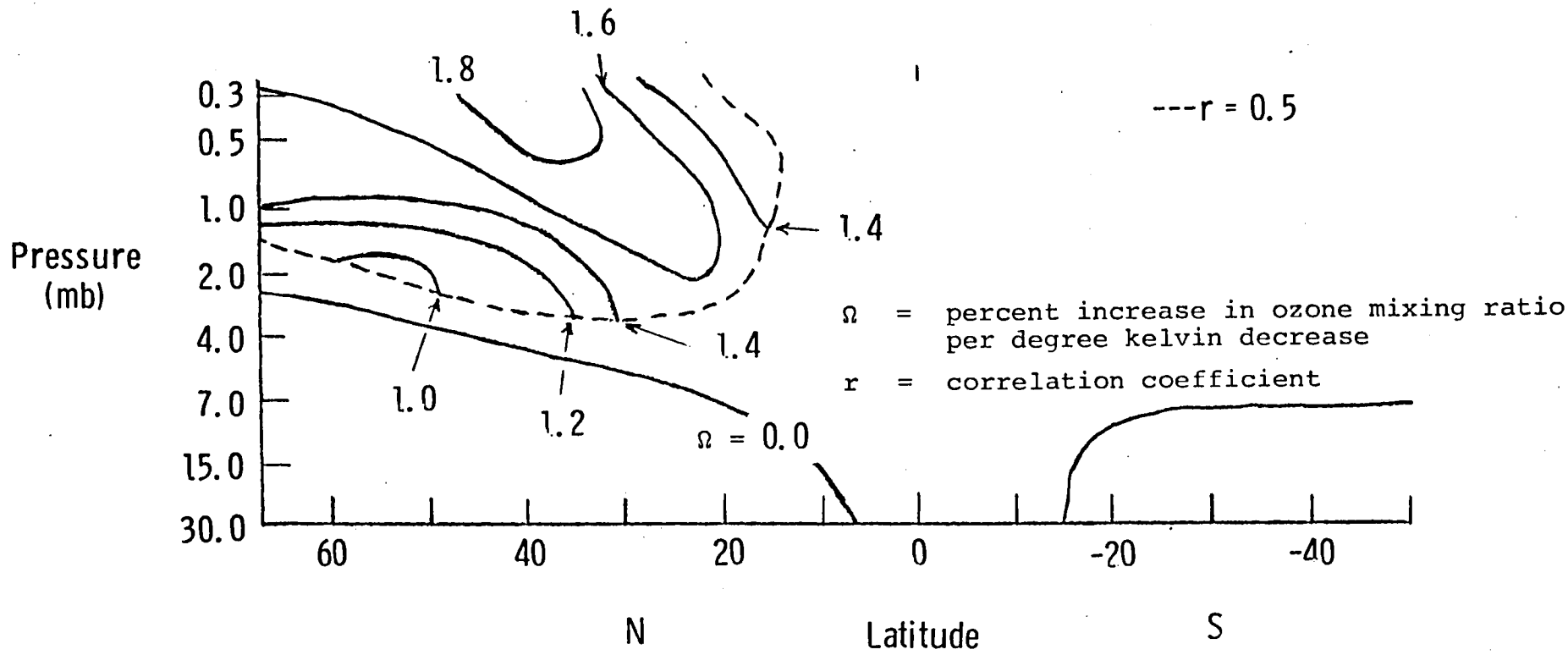

Figure 5. The percent increase in ozone mixing ratio per degree kelvin decrease in temperature (regression coefficients) as a function of latitude and atmospheric pressure for correlation coefficients $\geq$ -0.5 obtained from Nimbus 7 observations between December 24, 1978 and February 8, 1979.

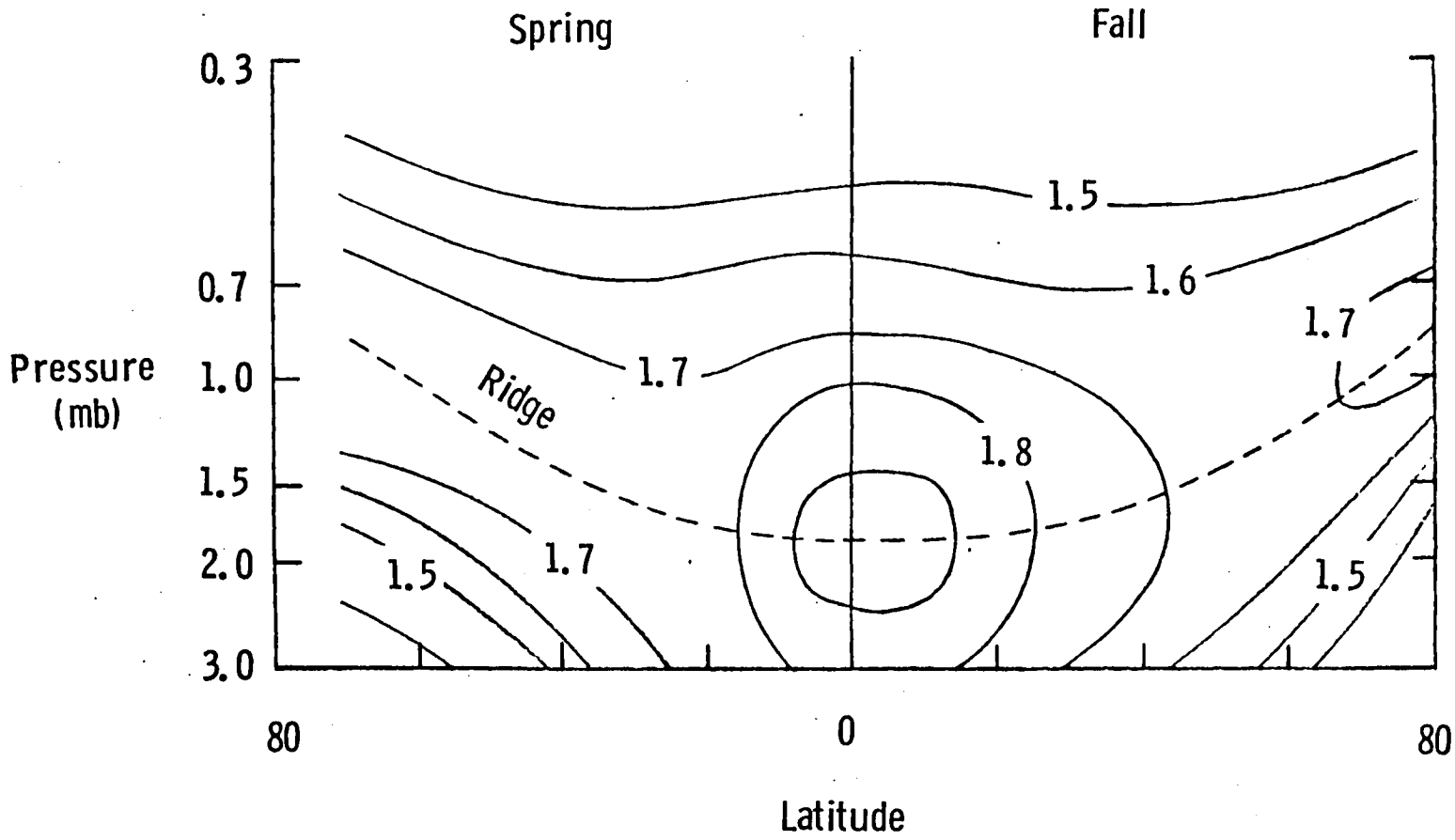

Figure 6. The calculated percent increase in ozone mixing ratio per degree kelvin decrease in temperature during Spring and Fall as a function of latitude and atmospheric pressure using the Pyle et al. theoretical model.

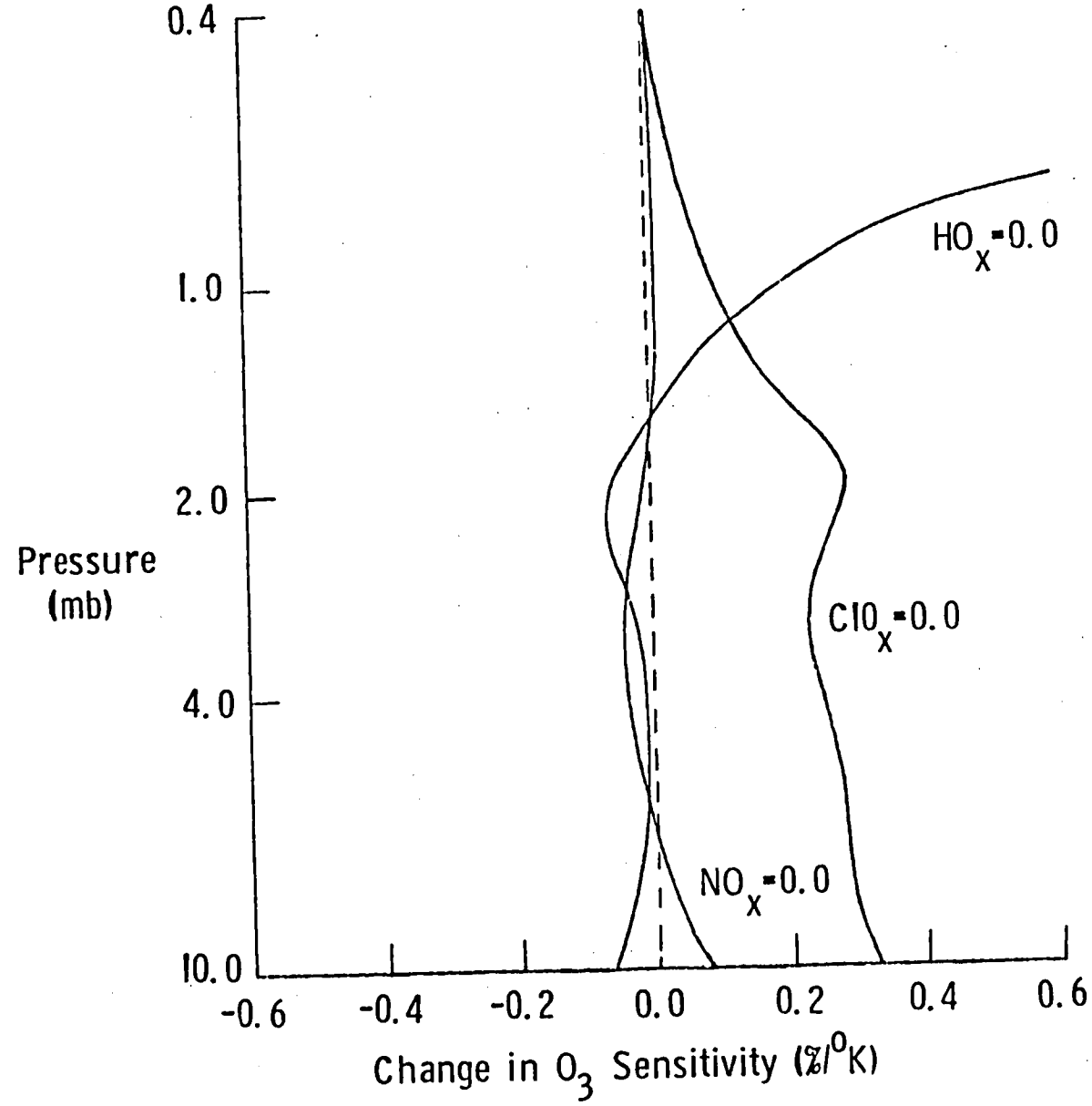

Figure 7. Calculated change in ozone sensitivity with atmospheric pressure from Pyle et al. model at the equator when loss terms for HO_x, ClO_x, or NO_x families are removed.

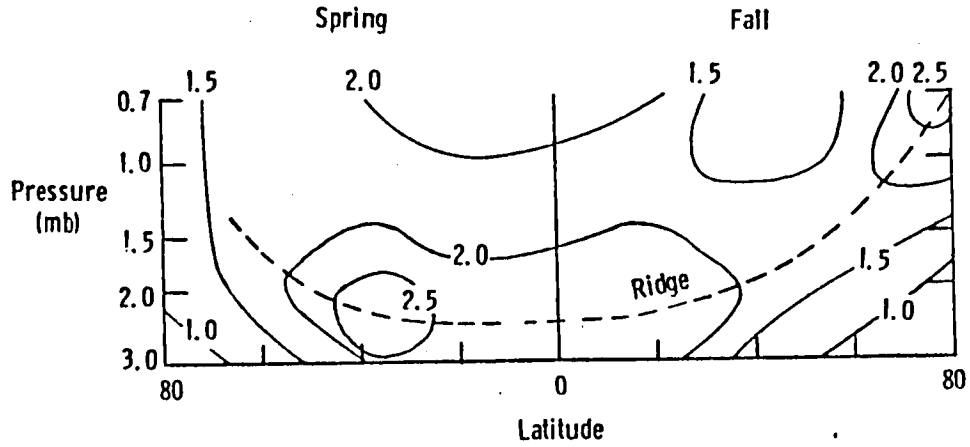

(a) Nimbus 4 observations

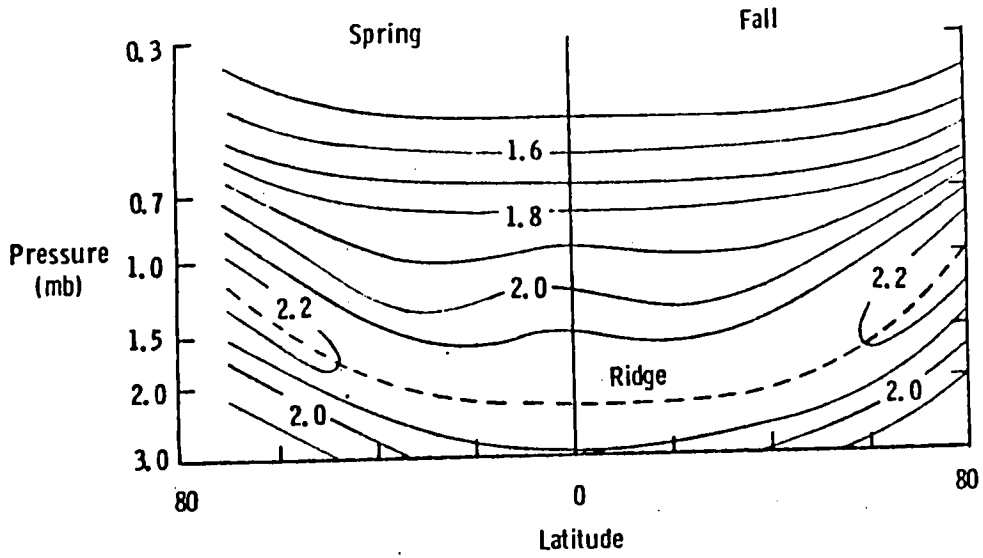

(b) Pyle model calculations with $C\ell O_x$ loss term removed.

Figure 8. Spring and Fall observed variation in the ratio of percent increase in ozone per degree kelvin decrease from the Nimbus 4 March-April and September-October observations and the Pyle model calculations with $C\ell O_x$ loss term removed as a function of latitude and atmospheric pressure.

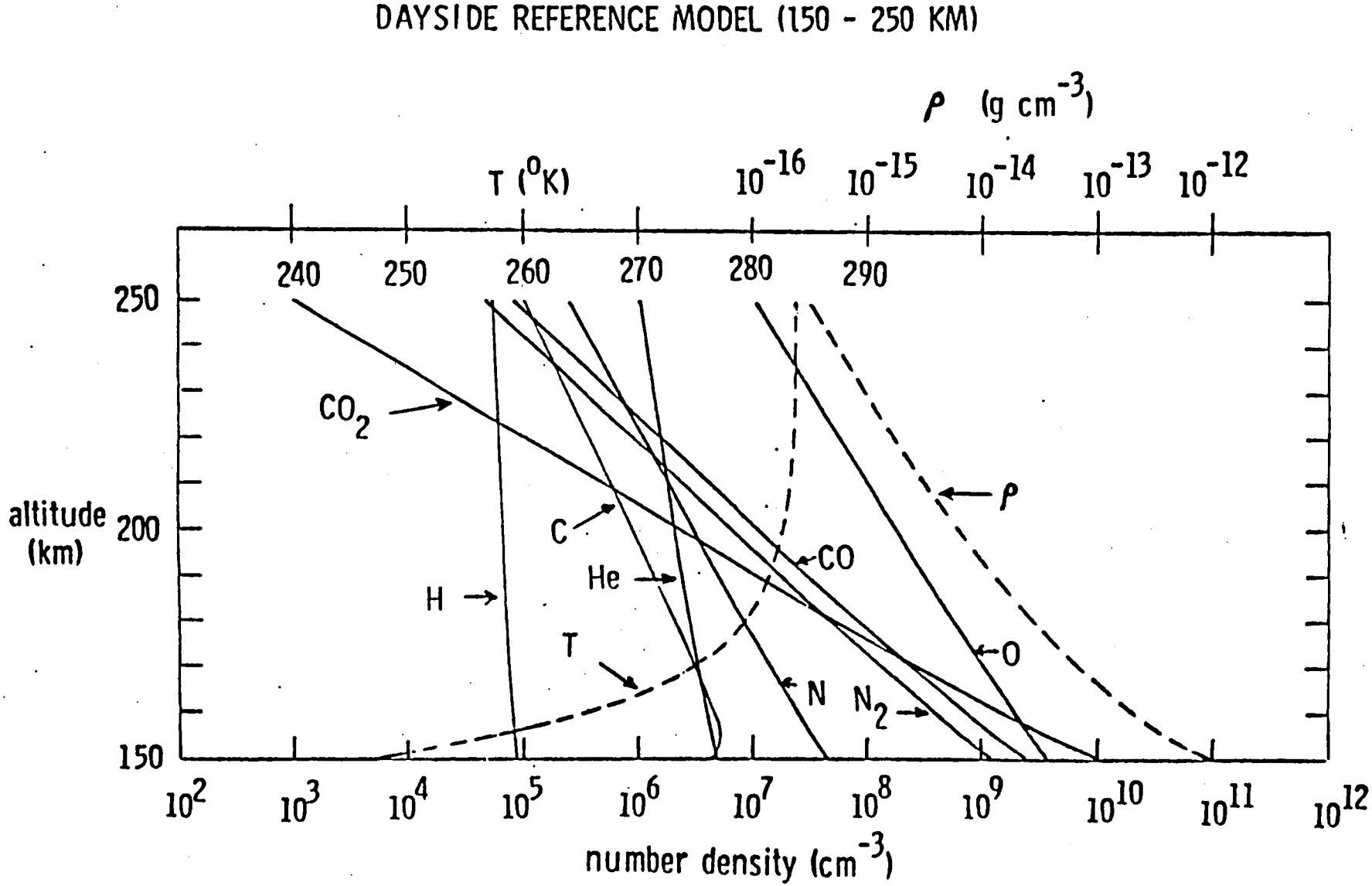

Figure 9. Variation of number density of CO_2, H, C, H_e, CO, O, N, and N_2, Temperature (T) and density (ρ) with altitude from the dayside reference model of Venus.

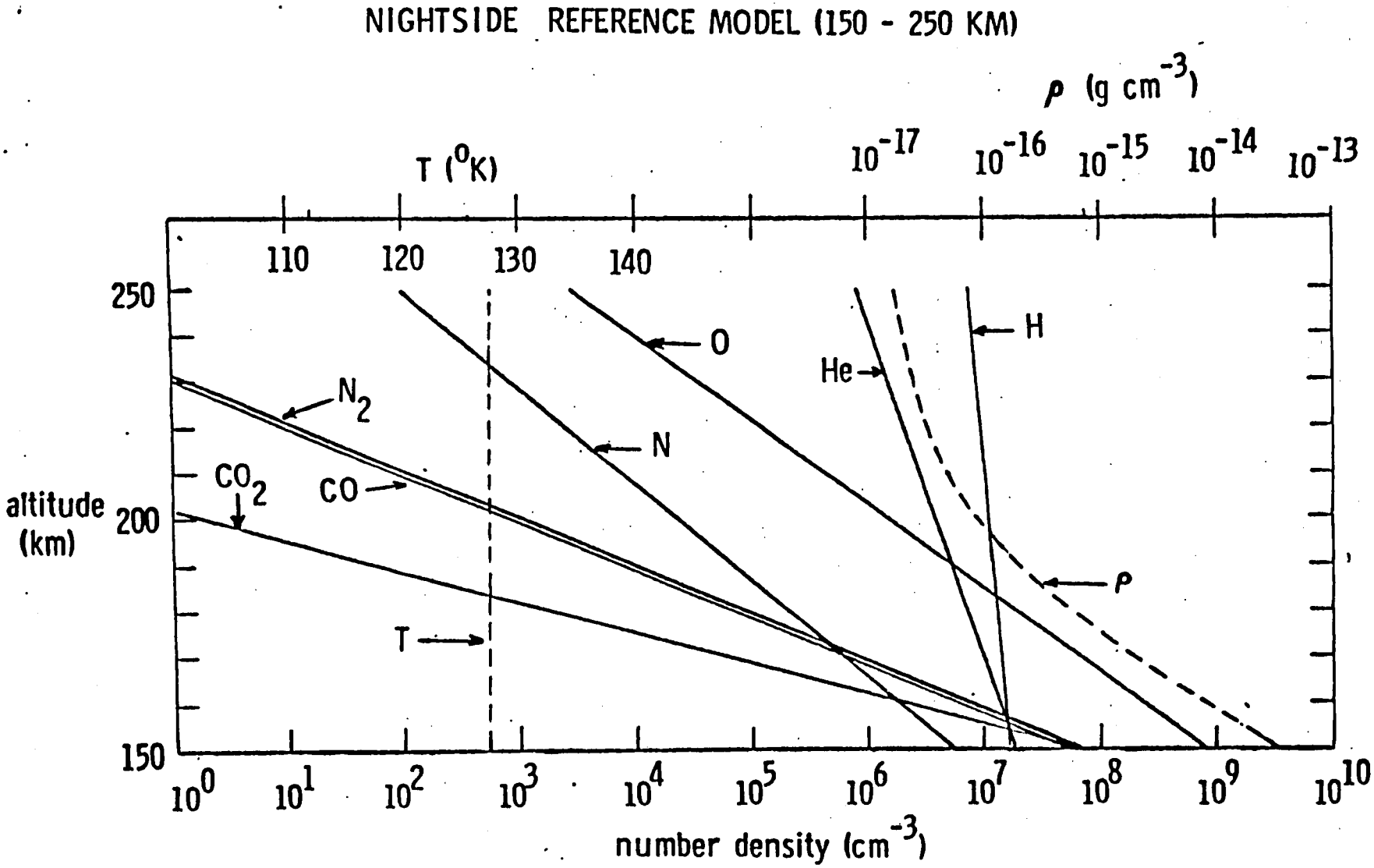

Figure 10. Variation of the number density of CO_2, H, C, H_e, CO, O, N, and N_2, Temperature (T) and density (ρ) with altitude from the nightside reference model of Venus.

1. Report No.	2. Government Accession No.	3. Recipient's Catalog No.
NASA CR-172437		

4. Title and Subtitle	5. Report Date
Empirical Studies of Upper Atmospheric Species	July 10, 1984
	6. Performing Organization Code
7. Author(s)	8. Performing Organization Report No.
J. Nicholson, M. Pitts & D. Young	
9. Performing Organization Name and Address	10. Work Unit No.
Systems and Applied Sciences Corporation 17 Research Drive Hampton, Virginia 23666	11. Contract or Grant No. NAS1-17089
	13. Type of Report and Period Covered
12. Sponsoring Agency Name and Address	Contractor Report
National Aeronautics and Space Administration Washington, DC 20546	14. Sponsoring Agency Code

15. Supplementary Notes

Langley Technical Monitor: Walter E. Bressette
Final Report

16. Abstract

The first month of SOI data (October 1981) has been processed and compared with TOMS and ground-based data. Short-term variations in the ozone field have been revealed using animated sequences of SOI data. High correlations have been observed between SOI ozone and upper tropospheric meteorological data. The relationship between ozone and temperature in the stratosphere has been investigated by examining Nimbus 4 BUV ozone and SCR temperature measurements as well as Nimbus 7 SBUV ozone and SAMS temperature measurements. Results from these ozone-temperature studies have been compared with calculations from theoretical 2-D models. All of the LIMS data has been processed at 10 pressure levels and correlations between various species have been performed. The Venus Atmospheric Drag (OAD) model has been modified taking into account recent investigations on the Venus thermosphere and the resulting model will be considered for incorporation into the Venus International Reference Atmosphere (VIRA).

17. Key Words (Suggested by Author(s))	18. Distribution Statement
upper atmospheric species ozone ozone-temperature relationship Venus minor species	Unclassified-Unlimited

19. Security Classif. (of this report)	20. Security Classif. (of this page)	21. No. of Pages	22. Price*
Unclassified	Unclassified		